Evaluation of the reactivity, selectivity and lifetime of hydrotalcite-based catalysts using isopropanol as probe molecule

Zoulikha Abdelsadek[1,2] · **Sergio Gonzalez-Cortes**[3] · **Feroudja Bali**[2] · **OuizaCherifi**[2] · **Djamila Halliche**[2] · **Patrick J. Masset**[4]

Abstract

Hydrotalcite catalysts derived from NiAl and NiAlMg mixed oxides were successfully prepared by coprecipitation at a constant pH of 11. Physicochemical methods were investigated to determine their structural and textural properties. Using isopropanol as a probe molecule, the acid–base properties of the catalysts were investigated, and the evaluation of reactivity, selectivity and lifetime was established.

Keywords Hydrotalcite · Structural characterization · Isopropanol probe reactions · Acid–base properties

Introduction

Hydrotalcite is the generic name for isomorphic compounds of general formula $Mg_6Al_2(OH)_{16} CO_3 \cdot 4H_2O$. Hydrotalcite-type anionic clays, layered double hydroxides (LDHs) containing exchangeable anions belong to materials that have attracted much attention in recent years. The structure of the layered double hydroxides can be visualized as the structure of brucite, $Mg (OH)_2$. The brucite phase is constituted

✉ Zoulikha Abdelsadek
   z.abdelsadek@univ-boumerdes.dz

✉ Patrick J. Masset
   patrick.masset@tu.koszalin.pl

1   Institute of Electrical and Electronics Engineering, University of M'hamed-Bougara, Independence Avenue, 35000 Boumerdès, Algeria

2   Laboratory of Chemistry and Natural Gas, Faculty of Chemistry, USTHB, El-Alia, B.P. 32, 16111 Bab-Ezzouar, Algiers, Algeria

3   Inorganic Chemistry Laboratory, Department of Chemistry, University of Oxford, South Parks Road, Oxford OX1 3QR, UK

4   Faculty of Mechanical Engineering, Koszalin University of Technology, ul. Śniadeckich 2, 75-453 Koszalin, Poland

of octahedrons with six OH^- groups each surrounded by Mg^{2+} ions. Sheets are then constituted by the replication of octahedrons. For derived hydrotalcite structures, a part of Mg^{+2} of the brucite is replaced by divalent and trivalent cations, where their atomic radius must be close to Mg^{2+} radius ($r = 0.65$ Å). The substitution leads to an excess of positive charges in the hydroxide layers, which are compensated by anions located in interlayer interspaces. The general chemical formula of LDHs is $[M_{1-x}^{2+}M_x^{3+}(OH)_2]^{x+}[A^{n-}]_{x/n}.mH_2O$, with M^{2+} and M^{3+} are divalent and trivalent metals, A^{n-} is an exchangeable interlayer anion such as CO_3^{2-}, NO_3^-, Cl^-…etc. and x is the molar fraction ratio $\frac{M^{3+}}{M^{3+}+M^{2+}}$, respectively. The value of x is an important parameter to obtain a pure hydrotalcite structure with a good crystallinity. It has been reported that this is obtained only in the range $0.2 \leq x \leq 0.33$. When x takes a value higher than 0.33, the gibbsite phase $Al(OH)_3$ forms. Likewise, for low values of x, i.e., $x < 0.2$, the brucite phase $Mg(OH)_2$ is stable [1, 2].

Different preparation methods of the hydrotalcites were investigated to tune their physical and chemical properties in order to apply them in specific applications. However, the coprecipitation process remains the best synthesis approach for the following reasons [3, 4]:

- Easy and friendly condition method,
- Cost-effective,
- High reproducibility,
- High production rate and easily scalable,
- Good dispersion of the active phase.

Several textural and structural properties of non-calcined and calcined hydrotalcite phases as nanomaterials have been applied in a wide variety of fields such as medicine, pharmaceutical, biotechnology, electronic, environment, catalysis and catalysts system (Fig. 1) [1].

Recently, oxides obtained by calcination of hydrotalcite have attracted much attention as catalytic system for applications, such as natural gas conversion and production of hydrogen by dry reforming of methane [5, 6], Friedel Craft reaction [7], methanol synthesis [8], etc. The calcination of hydrotalcites at sufficiently high temperatures leads to their dehydration, which is accompanied by de-hydroxylation and then decarboxylation reactions. It ends up with the collapse of the lamellar structure. In addition, mixed oxide phases are obtained at temperatures beyond 450 °C. The following properties can be highlighted from the combination of metal oxides [1, 6, 8–10]:

- Stable phases with a significant specific surface (between 100 and 300 m^2/g),
- Tunable acidic/basic and redox properties,
- Homogeneous dispersion of the active phase.

The catalytic activity and selectivity of the catalyst are closely related to its acid–base, redox properties, textural and structural features resulting from the synthesis conditions. Several probe molecules like CO_2 and NH_3 were used to
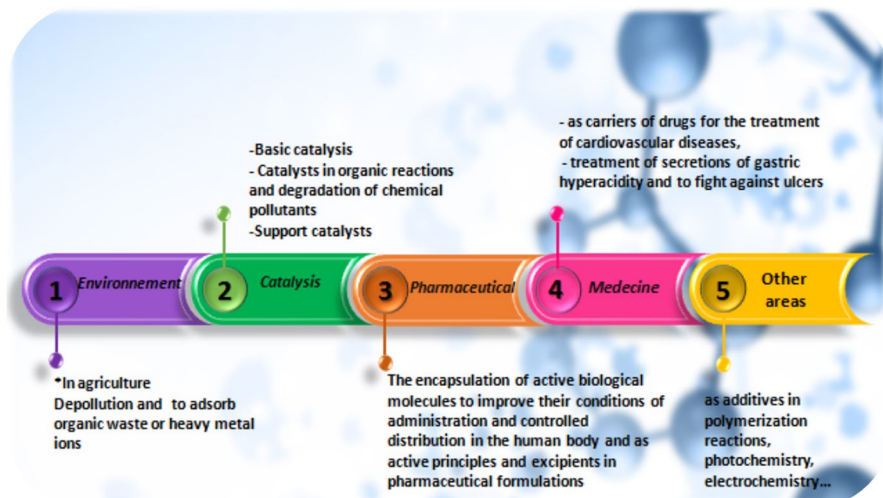
Fig. 1 Different applications of hydrotalcite

characterize the basic and acidic properties of the solids surface, respectively. The conversion of alcohol as catalytic test reaction has been intensively investigated and used to characterize and evaluate the acid–base character of solid catalysts [11, 12]. Most of the attention has been paid to targeted molecules (e.g., isopropanol) that are transformed into products depending on the nature of the available reactive centers onto the heterogeneous catalyst surface. Such reactions have the advantage of being simple and easy to be followed through the quantification of conversion rates. In addition, it can be performed at relatively low temperatures. In contact with an acidic or basic solid, the isopropanol probe molecule may undergo mainly two types of competitive elimination reactions: (i) dehydration, which yields propylene and takes place on acid sites of the catalyst. The formation of di-isopropyl is also possible as a product of the dehydration of propylene and (ii) dehydrogenation reaction produces acetone and hydrogen and occurs in basic sites [13–15] (Fig. 2). The yield and selectivity of products for isopropanol transformation depend on the acid–base features of catalytic surface, which constitutes a well-suited probe molecule in the design of advanced catalysts.

For each application, especially for catalysis applications, the acid–base properties of the catalysts are key parameters regarding their reactivity, selectivity and lifetime. There is strong incentive to enhance solid base properties of catalysts in order to improve their catalytic activity for reactions, such as alkylation, isomerization and Knoevenagel condensation reaction under specific friendly experimental conditions. Materials like zeolites, alkaline earth, basic resin, nickel ferrite spinel, oxides (ZnO, MgO), vanadium-containing catalysts and modified carbon have already been investigated for these reactions and isopropanol transformation [16–18].

Recently, there has been a great interest in the utilization of oxides obtained from calcined hydrotalcites due to their promising strong base properties [1, 10]. The catalytic properties of oxides derived from hydrotalcite depend mainly on the nature of
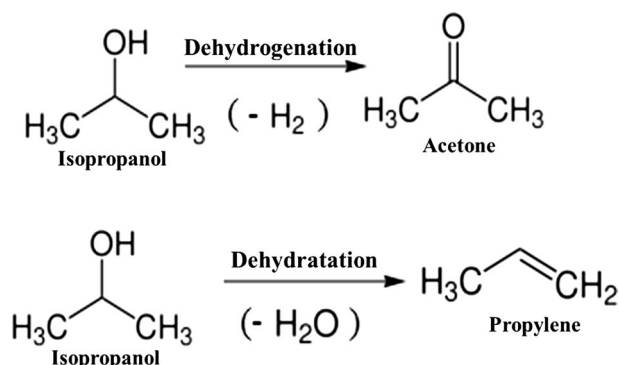
Fig. 2 Pathway of the isopropanol decomposition

divalent and trivalent cations, exchangeable interlayer anions and chemical composition of the hydrotalcite structure and on the activation process which requires acid, base and redox active sites. The decomposition mechanism provides a valuable test reaction to investigate the acid–base properties of materials. Hereafter, the role of Mg is emphasized in reference to its use in hydrotalcite-based catalysts.

Nakatsuka et al. [19] investigated the activity of calcination products of several MgAl-HTc in the polymerization of ß-propiolactone. All the HT precursors were calcined at 450 °C for one hour. According to the authors, MgO prepared by calcination was not active in the reaction. Moreover, a correlation was found between the activity and the number of basic sites. The inhibition of activity occurring upon CO_2 and H_2O additions confirmed the role of the basic sites in the formation of the polymerization centers. In particular, the authors correlated the activity to the interaction between MgO and Al_2O_3, favoring the formation of suitable basic sites. The basic character was examined for the first time on the compound MgAl-CO_3-HT, the heat treatment of which allows to obtain oxides of the MgO type [1, 10]. The basic properties of MgO have been widely studied in the literature [1, 20]. Strong basic sites are assigned to O^{2-} species, while medium basic sites are assigned to (O^-) groups located near hydroxyl groups. The low basicity is attributed to the (OH^-) group (Brønsted basicity).

As a conclusion, the activity of MgAl pure, after calcination at 450 °C, the XRD analysis showed the presence of mixed oxides: MgO with Al_2O_3. The catalytic activity behavior of this sample via isopropanol decomposition is to produce acetone through strong basic sites [21]. In addition, the combination of MgO-Al_2O_3 promotes the formation of suitable basic sites [1]. The number of defects, and therefore the number of strong basic sites, in the lattice of MgAl should be expected to increase when increasing the amount of Al introduced. Since Al is more electronegative than Mg, an increase in Al should increase the average electronegativity of the solid and thus, a decrease in the average electronic density of the unsaturated framework oxygen could be expected reflecting in the basic strength [22].

On the other hand, the propylene formation on the MgAl hydrotalcite sample can be related to the presence of acid sites associated with Al^{3+}, which is substituted by Mg^{2+}

in a MgO lattice. This substitution may produce local excess of positive charge in the lattice of the oxide which can act as acid sites [22].

The NiAl-HT- and NiMgAl-HT-type hydrotalcite have been studied in many applications such as Friedel craft reaction, aldolization and dry reforming of methane [1, 6]. For the last process, researchers suggest that the basic properties of catalyst derived from hydrotalcite improve the catalytic activity, CO_2 activation and consequently the resistance of carbon deposition [1, 23].

In the present work, mixed oxides catalysts derived from hydrotalcite of samples NiAl-HTc and NiMgAl-HTc were prepared by coprecipitation method, characterized by different chemical–physical techniques and tested in the isopropanol decomposition reaction. The purpose of this work is to evaluate the effect and the influence of the presence of Mg in HDL matrix on textural and structural catalytic properties and acid–base properties of mixed oxides nanomaterials derived from hydrotalcite. The use of isopropanol as probe molecule was considered as a low temperature method under 250 °C, where no structural changes are expected (as it is the case for TPR analysis) and allow the investigation of the composition and especially the use of substitutes of Ni by Mg and Al.

Experimental

Sample preparation

The catalysts obtained from the hydrotalcite calcined type precursors were prepared by coprecipitation by mixing two solutions: i) a solution containing divalent cations Ni $(NO_3)_2 \cdot 6H_2O$ (Merck, 99%) or with Mg $(NO_3)_2 \cdot 6H_2O$ (Merck, 99%), and trivalent cations Al $(NO_3)_3 \cdot 9H_2O$ (Fluka, 98%) ii) a solution prepared by dissolving an amount of Na_2CO_3(Merck, 98%) and NaOH (Merck, 98%) to adjust the pH. The two solutions were mixed dropwise under vigorous stirring at room temperature and at pH basic constant (pH 11). The final pH of the total solution was adjusted by adding NaOH solution (2 M). After the addition of reagents, the obtained gel was aged at 80 °C in oil bath shaker for 18 h under gentle stirring. The solid was cooled to room temperature, then filtered and washed with a large amount of deionized water to remove all residuals until getting a solution pH equal to 7. The resulting slurry was dried overnight by an oven at 80 °C under air. The non-calcined synthesized samples were labeled NiAl-$CO_3$and NiMgAl-CO_3.

After drying, the solids NiAl-$CO_3$and NiMgAl-CO_3 were calcined at 450 °C for 6 h using a heating rate of 4 °C/min in a muffle furnace. The calcined materials obtained were referred to NiAl-CO_3-c and NiMgAl-CO_3-c. The solids were crushed to obtain a fine powder (Fig. 3).
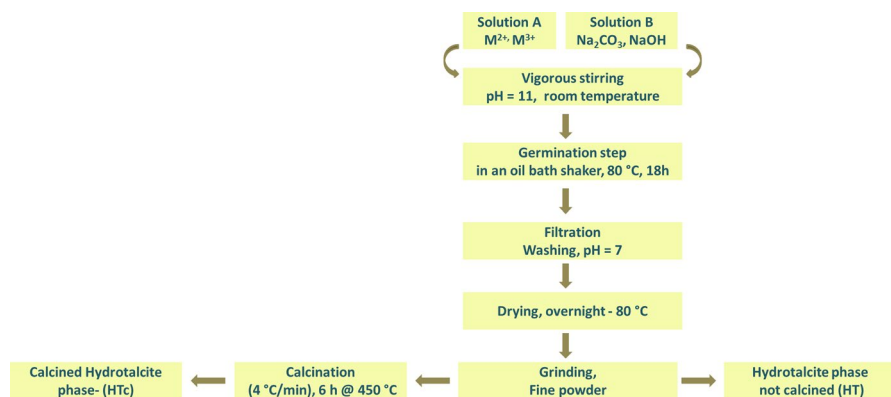
Fig. 3 Scheme of HDLs synthesis

Sample characterization

Atomic absorption spectroscopy (AAS) analysis

The chemical composition was determined by Atomic Absorption Spectroscopy (AAS) using Spectro-Analytical Instruments Horiba Jobin–Yvon, Ultima spectrometer; 100 mg of the solids was dissolved in 20 ml of aqua regia and the solution was diluted to 100 ml with distilled water.

X-ray diffraction (XRD) analysis

Powder X-ray diffraction (XRD) patterns were recorded with Siemens D-501 equipment, using CuK_α *radiation* in the 2θ range between 10 and 80°. The crystallite size was evaluated using the Scherrer's formula [Eq. (1)] [24, 25].

$$d_{hkl} = \frac{0.9\lambda}{\beta_{hkl}\cos\theta} \tag{1}$$

where λ is the wavelength of $CuK\alpha$ ($\lambda = 1.5418$ Å), β_{hkl} is the half-width of the peak, and θ is the Bragg's diffraction angle.

Brunauer–Emmett–Teller (BET) analysis

Brunauer–Emmett–Teller (BET) surface area measurements were carried out using a NOVA 2000e volumetric adsorption analyzer at -196 °C (liquid nitrogen). Before each measurement, the powder was degassed under vacuum at 150 °C for 2 h.

Fourier transform infrared (FTIR) analysis

Fourier transform infrared (FTIR) spectra were recorded using a Perkin Elmer model number spectrometer. Over 32 scans were taken to improve the signal-to-noise ratio in the wavelength range (400–4000 cm^{-1}) with a resolution of 4 cm^{-1}. The analysis was performed on *ca*. 4 mg of powder mixed with 100 mg of dried spectroscopic KBr pressed into pellets.

Thermogravimetry analysis (TG) and differential thermal analysis (DTA)

Thermogravimetry analysis (TGA) and differential thermal analysis (DTA) were performed using a Netzsch STA 409 PC/PG instrument under air as purge gas from room temperature up to 850 °C with a heating rate of 10 °C/min using alumina crucibles.

Scanning electron microscopy analysis (SEM)

Scanning electron microscopy images (SEM) of the products were recorded on a Hitachi S-4800 instrument equipped with a field emission filament using an acceleration voltage of 5 kV and a working distance of 10 mm.

Transmission electron microscopy analysis (TEM)

A transmission electron microscopy (TEM) study of the samples was carried out at 200 kV using a Philips CM200 TEM equipped with a LaB6 emitter, an Oxford ISIS EDX super-ultrathin window detector and a Gatan Model 678 Imaging Filter (GIF). The crushed sample dispersed in ethanol solution was vigorously stirred using ultrasound to minimize the deposit of clusters of particles. A droplet of this suspension is then placed on a copper grid covered with a carbon film. Once the grid is ready; SEM analysis can be measured.

Catalytic testing

The isopropanol decomposition on material catalysts takes place through two pathways: the dehydration, which generally needs acid catalysts or the two types of acidic–basic sites, dehydrogenation is catalyzed by basic sites.

The catalytic tests of transformation of isopropanol (Merck, 99.7%) were conducted in a fixed bed continuous flow reactor under atmospheric pressure and temperature between 150 and 250 °C, by passing nitrogen gas through a saturator-containing alcohol. The mass of catalyst was approx. 0.02 g, and the flow rate was kept to 0.05 ml/min. The tests were carried out at atmospheric pressure and the saturating vapor of the gaseous propan2-ol reagent ($P_0 = 4$ mmHg) is obtained by bubbling nitrogen (380 mmHg) in liquid propan2-ol placed in a saturator immersed in an ice bath.

Reactants and reaction products were analyzed by gas chromatography (VARIAN 3350) using a 10% Carbowax 20 M on Chromosorb 200 column and flame ionization detector.

The conversion of isopropanol (Con_{isop}), selectivity of propene (Sec_{prop}) and selectivity of acetone (Sec_{acet}) were estimated using the following formulas:

$$Con_{isop}(\%) = \frac{\text{Moles of isopropanol converted}}{\text{Moles of isopropanol in feed}} \times 100$$

$$Sec_{prop}(\%) = \frac{\text{Moles of propylene produced}}{\text{Moles of isopropanol converted}} \times 100$$

$$Sec_{acet}(\%) = \frac{\text{Moles of acetene produced}}{\text{Moles of isopropanol converted}} \times 100$$

Results and discussion

Characterization of catalyst

The chemical formula of the synthesized samples was determined by X-ray fluorescence supposing that the carbonates are the only anions in the inter-layer. The number of the carbonates was estimated from the molar ratio M^{2+}/M^{3+}. The water molecules content (mH_2O) was calculated using the formula (Eq. 2):

$$18m = \frac{w(a + 18m)}{100} \tag{2}$$

where m is the number of water molecules in the inter-lamellar space, a is the molecular mass of the anhydrous compound and w the mass loss (%) of water derived from the thermogravimetric analysis (Fig. 4).

The data of the X-ray fluorescence technique (Table 1) confirm that the M^{2+}/M^{3+} ratios were like those estimated from the concentrations of the salts in the initial synthesis solution. This result confirms the complete precipitation of Ni/Mg and Al precursor salts during the synthesis. The results confirm the presence of the transition metals used (Ni, Mg and Al) in all hydroxides double lamellar phase (HDL-phases) samples. This indicates that the operating conditions such as the pH, precipitating agent, temperature of the germination phase lead to the precipitation of divalent and trivalent ions under stoichiometric conditions.

The result obtained (Table 1) indicates that the general formula $[M_{1-x}^{2+}M_x^{3+}(OH)_2]^{x+}[A^{n-}]_{x/n} \cdot mH_2O$ enables the synthesis of HDL-phases with different divalent and trivalent metals where $0.22 \leq x \leq 0.33$ [1, 6, 26]. The mass changes of the samples type hydrotalcites were derived from TGA/DTA analyses. The analysis showed the typical results reported in the literature of the thermal decomposition of hydrotalcite as materials [1, 6, 27]. According to Table 2 and
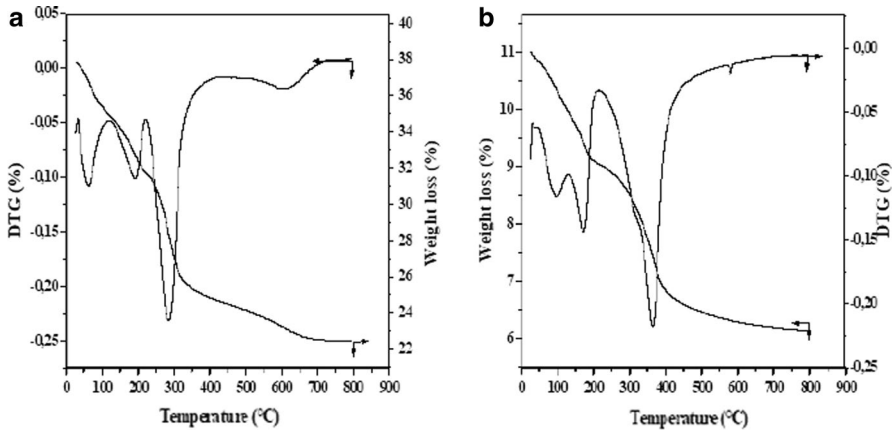
Fig. 4 TGA/DTA for **a** NiMgAl-CO$_3$ and **b** NiAl-CO$_3$

Fig. 2, the evolution of the thermal decomposition of hydrotalcite phases reveals three steps of the mass losses. The first step presents the moving of the physically absorbed molecules on the outer surface of the HDL-phases at 100 °C corresponding to 4 and 5 wt% for NiMgAl-CO$_3$ and NiAl-CO$_3$, respectively. The second step designs the elimination of inter-lamellar water by de-hydroxylation phenomena accompanied by the elimination of nitrates molecules at around 200–205 °C accounting 15–16 wt%.The third and the last step occurs at higher temperatures (300–320 °C), which is characterized by the elimination of the carbonates in the layer space with mass loss corresponding to 35 and 31 wt% for NiMgAl-CO$_3$ and for NiAl-CO$_3$, respectively.

The BET surface area (S_{BET}) non-calcined and calcined specimens at 450 °C materials are summarized in Table 2. For the two samples, the surface area after

Table 1 Chemical composition of the prepared samples

Sample name	$x = \frac{n M^{3+}}{n(M^{2+}+M^{3+})}$	ratio $\frac{M^{2+}}{M^{3+}}$	MgO (%) (%)	NiO (%)	Al$_2$O$_3$ (%)	Formula
NiMgAl-CO$_3$-c	0.33	1.97	26.19	23.19	32.96	[Ni$_{0.22}$Mg$_{0.45}$Al$_{0.33}$](CO$_3$)$_{0.165}$·0.15H$_2$O
NiAl-HT-CO$_3$-c	0.34	1.91	–	67.28	24.56	[Ni$_{0.65}$Al$_{0.34}$](CO$_3$)$_{0.170}$·0.24H$_2$O

Table 2 TG results and specific surface of two prepared samples

Sample	First stage		Second stage		Third stage		S_{BET} (m^2/g)	
	Wt%	Temperature (°C)	Wt%	Temperature (°C)	Wt%	Temperature (°C)	Precursor	Calcinated
NiMgAl-CO$_3$	4	100	16	205	35	320	94	169
NiAl-CO$_3$	5	100	15	200	31	300	32	117

calcination is greater than the precursor. This result is due to the occurrence of three phenomena: dehydration, de-hydroxylation and decarbonation during thermal treatment. The sample contains Mg (i.e., NiMgAl-CO$_3$) and shows high specific area after and before calcination compared to NiAl-CO$_3$ due to dispersive effects, which have already been investigated and reported in the literature [1, 9, 28].

Usually, a high surface area leads to a good catalytic activity due to the high dispersion of active phase. In the present work, non-calcined NiMgAl-HT and even after calcination exhibits a large surface area compared to calcined and non-calcined NiAl-HTc. This result is explained by the incorporation of Mg into NiAl hydrotalcite matrix. The presence of Mg2 + cation increases the specific surface area and modifies the pore diameter. Furthermore, the crystallite size's phase presented by NiMgAl-HTc resulted smaller than that for NiAl-HTc as confirmed by XRD analysis. This result agrees with previous findings from Crivello et al. and Abdelsadek et al. [28, 29] who determined that the Mg^{2+} cation has a dispersive effect over the other components of the catalyst. In the case of the solid NiMgAl-HTc, a great activity or catalytic behavior was obtained with larger surface area influence for the isopropanol decomposition and dry reforming of methane [29].

Figure 3 shows the XRD patterns of HDL precursor phases and calcined samples. The diffractograms of the precursor samples NiMgAl-CO$_3$ and NiAl-CO$_3$ show the presence of two main peaks allocated to the layered double hydroxides phases of hydrotalcite: peaks intense sharp symmetric reflections for (003), (006), (110) and (113) planes and asymmetric broad peaks for (012), (015) and (018). No other phase was detected which indicates that the divalent and trivalent ions were completely introduced into hydrotalcite structure under the selected experimental conditions. This enables synthesizing hydrotalcite phases with mixtures of different divalent and trivalent cations in the right range of metallic composition. After calcination at 450 °C, the XRD patterns (Fig. 5) show clearly that the structure was modified. The hydrotalcite phases were decomposed to form metallic oxides. The NiO phase was detected for the NiMgAl-CO$_3$-c and NiAl-CO$_3$-c
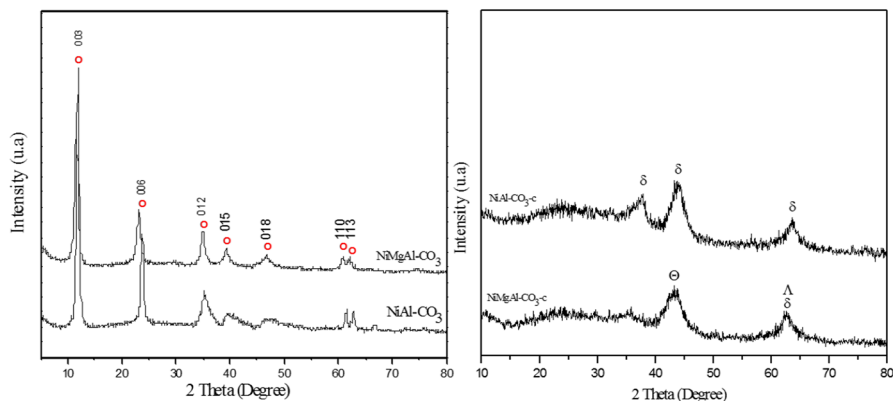

Fig. 5 X-ray diffractograms of precursor NiMgAl-CO$_3$ and NiAl-CO$_3$ and calcined sample NiMgAl-CO$_3$-c and NiAl-CO$_3$-c. (o): HDL phase, δ NiO, Λ MgO and Θ NiO-MgO
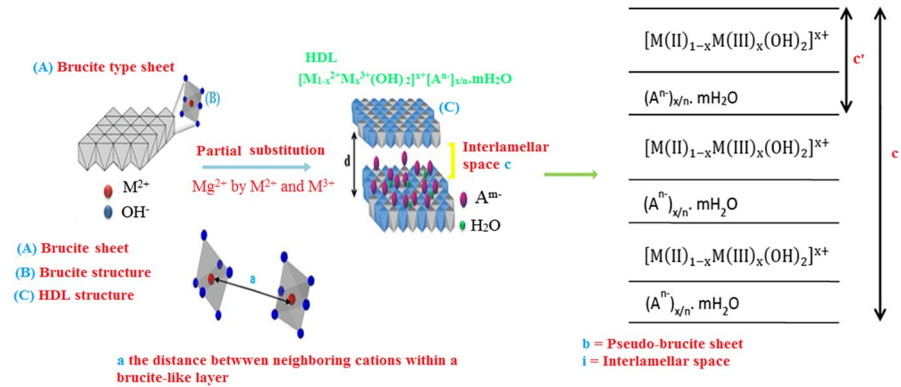
Fig. 6 HDL structure and structural parameters a and c

Table 3 Crystallographic parameter a and c with crystallite size of synthesized HDL

Sample name	d_{003} (Å)	$c = d_{003}$ (Å)	$a = 2d_{110}$ (Å)	Crystallite size' phases (Å)			
				003[a]	110[a]	MgO	NiO
NiMgAl-CO$_3$	7.60	22.74	3.04	95	110	22	25
NiAl-CO$_3$	7.70	22.96	3.04	156	208	–	35

[a]Hydrotalcite phase

calcined samples, plus MgO in the case of NiMgAl-CO$_3$-c. However, alumina Al$_2$O$_3$ was probably formed but was not detected by XRD analysis since it is an amorphous phase at this temperature. No ternary or mixed oxides were detected by XRD analysis.

The first reflection of the plane (003) is characteristic of the successive stacking of the layers along the axis c. The mesh parameter (c) is easily calculated since it is equal to 3c′(c′ corresponding to the sum of the thickness of a layer of brucite (4.8 Å) and the inter-lamellar domain, i.e., the inter-reticular distance family plans (003). The mesh parameter (a) corresponds to the distance between neighboring cations within a brucite-like layer and is defined from the distance ($a = 2 \times d110$). The a and c parameters obtained for the HDL synthesized phases are very similar to the value reported in the literature [1, 4, 30] (Fig. 6).

The d$_{003}$, which presents inter-lamellar distance calculated for the carbonates hydrotalcite phases prepared samples is close to the value published (7.8 Å) [1, 31]. The crystallite size in a direction and c direction for the two materials is presented in Table 3.

The results obtained show that the dimensions in the a-direction are larger than that in c-direction which reveals the plate-like form of the hydrotalcite crystal phase. After calcination, the estimation of the crystallite sizes of the oxides NiO and MgO was estimated and is provided in Table 3. The crystallite sizes of the oxides (NiO, MgO) are lower than HDL precursor phase. It explains that the specific surfaces of
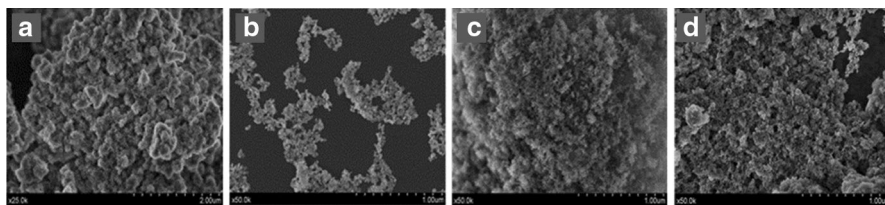
Fig. 7 SEM images of NiMgAl-CO$_3$ (**a**, **c**) and NiAl-CO$_3$ (**b**, **d**) with a, b: non-calcined phases and c, d: calcined phases
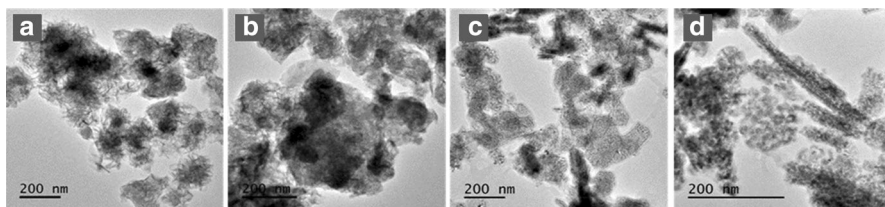
Fig. 8 TEM images of NiMgAl-CO$_3$ (**a**, **c**) and NiAl-CO$_3$ (**b**, **d**) with a, b: non-calcined phases and c, d: calcined phases

the calcined samples NiMgAl-CO$_3$ and NiAl-CO$_3$ are larger than the HDL precursor phases (Table 2). In addition, compared to the two solids NiMgAl-CO$_3$ and NiAl-CO$_3$, the non-calcined and calcined NiMgAl-CO$_3$ show high surface area than non-calcined and calcined NiAl-CO$_3$. Magnesium influences the germination and crystal growth step and leads to the formation of the nano-sized crystallites, fine small particles and also increases the specific surface of the compound [28, 32]. This result agrees with the results obtained by BET analysis (Tables 2 and 3).

The morphology of the samples prior to calcination was investigated by SEM and TEM analyzes. Figures 7 and 8 show the SEM and TEM images, respectively, of HDL phases synthesized for the samples non-calcined NiMgAl-CO$_3$ and NiAl-CO$_3$. SEM and TEM images of the NiAl-CO$_3$ show that the morphology of HDL phases prepared precursor confirms the presence and accumulation of fine nanoparticles of regular shape with inter-platelet porosity. The corresponding micrograph of the compound NiMgAl-CO$_3$ exhibits special features. It seems that the fine particles aggregate and connect to each other giving rise to a specific arrangement like a «rose sand» (Figs. 7a and 8a). This result was confirmed by the SEM images of this sample. Fine particles evidenced by SEM and TEM techniques correspond only to hydrotalcites phases precursor. This observation agrees with the results obtained by XRD analysis.

After calcination, the SEM (see Fig. 7c, d) and TEM (see Fig. 8c, d) images for the two calcined materials NiMgAl-CO$_3$-c and NiAl-CO$_3$-c show the presence of the compact aggregates owing to the transformed hydrotalcite structure during thermal treatment. These aggregates are related to the mixture of oxides phases as revealed by XRD analysis (see Fig. 3, Table 3). FTIR spectra of non-calcined NiMgAl-CO$_3$ and NiAl-CO$_3$ specimens are shown in Fig. 9a. The spectrum of the
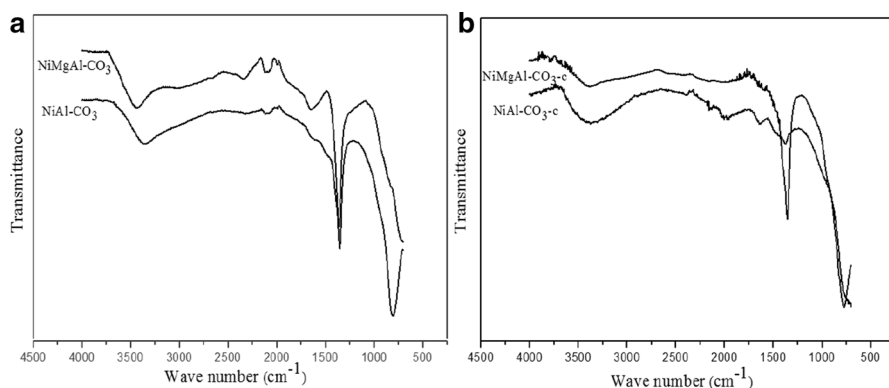
Fig. 9 Infrared spectra of **a** non-calcined and **b** calcined samples NiMgAl-CO$_3$-c and NiAl-CO$_3$-c

two non-calcined samples exhibits typical features of the non-calcined hydrotalcite phases non-calcined already reported in the literature [33]. Table 4 summarizes the different vibration bands before and after calcination of the solids NiMgAl-CO$_3$ and NiAl-CO$_3$.

After calcination, the decrease in the all intensities of the different bands was observed owing to the treatment thermal at 450 °C: dehydration, de-hydroxylation and decarbonation (Fig. 5b, Table 4). It notices the presence of vibration bands at 1380 cm^{-1} characteristic to the carbonates. These are the trace amounts of the remaining carbonates which are called «residual carbonates» and they are responsible for memory effect, specific properties of hydrotalcites materials calcined at temperature $\leq$ 450 °C [1, 34]. This result is in good agreement with the XRD data.

Raman assignment peaks (Fig. 10) of synthesized materials showed the same behavior to HDL phases structure described in literature reports [35] (Fig. 10). Broad stretching vibrations assigned at 3400–3600 cm^{-1} are attributed to OH vibrations of physisorbed water molecules. Stretching vibrations modes at 2447 and 2441 cm^{-1} for both solids NiMgAl-CO$_3$ and NiAl-CO$_3$, respectively, are associated with vibrations of OH units with metal. Raman bands at 1650 cm^{-1} for NiAl-CO$_3$ and 1654 cm^{-1} for NiMgAl-CO$_3$ are ascribed to inter-lamellar water deformation mode. The bands at 671 cm^{-1} (NiAl-CO$_3$) and 702 cm^{-1} (NiMgAl-CO$_3$) are designated to the γ_4CO$_3$ in the interlayer. The others bands (545, 404 and 364 cm^{-1}) for NiAl-CO$_3$ and (553, 450, 396, and 348 cm^{-1}) for NiMgAl-CO$_3$ are considered to the linkage Al–O–Al, Al–O–Ni in the two solids NiMgAl-CO$_3$ and NiAl-CO$_3$ in addition Al–O–Mg in the sample NiMgAl-CO$_3$.

Catalytic testing results

Isopropanol is a test molecule often used to detect acid–base features of materials and especially of catalysts. The transformation of isopropanol can lead to essential products such as acetone, propylene and in a lower degree di-isopropyl ether. The production of acetone by isopropanol dehydrogenation is related to the presence

Table 4 Summary table of the vibration bands characteristic of hydrotalcite-type materials before and after their calcination

Vibration bands (cm^{-1})	Matching group *Prior calcination*	Vibration bands (cm^{-1})	Matching group *After calcination (450 °C)*
3300–3500	H–O–H intercalated or adsorbed Stretching vibration	3300–3600	H–O–H, H$_2$O–OH, H$_2$O–CO$_3^{2-}$
1623	H–O–H inter-lamellar Bending vibration	1380	O–C–O (carbonate ions from the air)
1380	O–C–O (carbonate ions), vibration	764	M–O–M, M(II) or M(III)
1000	M–OH, translation	–	–
807	M–O–M, M(II) or M(III), vibration	–	–
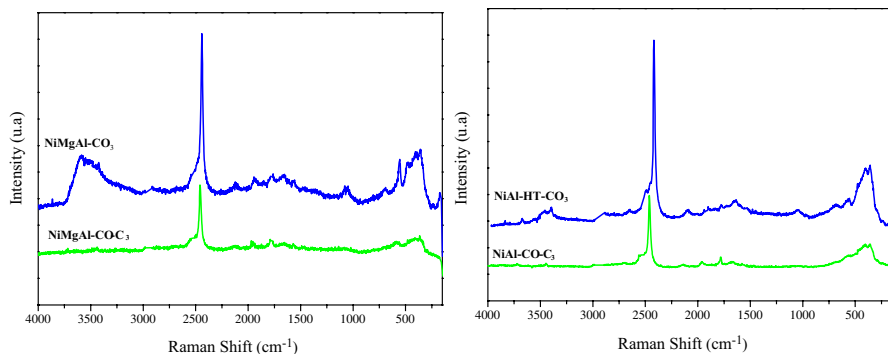
Fig. 10 Raman spectra of non-calcined (NiMgAl-CO$_3$ and NiAl-CO$_3$) and calcined samples (NiMgAl-CO$_3$-cand NiAl-CO$_3$-c)

of basic sites, whereas the formation of propylene occurs via acid sites (Fig. 2). The results of isopropanol conversion, selectivity into acetone and propylene were investigated at different temperatures over the two catalysts NiMgAl-CO$_3$-c and NiAl-CO$_3$-c and the results are depicted in Fig. 11.

According to the experimental results, both catalysts show a good catalytic activity for the isopropanol decomposition with different acid–base, redox properties depending on the composition of the samples NiAl-HTc and NiMgAl-HTc and support the presence of Mg in NiAl-HT matrix. Without minimizing the role of Ni in the catalytic properties of hydrotalcites especially for methane reforming process (dry reforming, vapor-reforming and oxidation) [1, 36, 37], it must be emphasized that NiMgAl-HTc exhibits a greater catalytic activity despite its lower amount of Ni relative to NiAl-HTc. Interestingly, NiAl-HTc also presents basic properties. Acetone is the major product for NiAl-HTc and NiMgAl-HTc catalysts; however the last formulation favors this product owing to the presence of Mg^{2+} cation. This result is consistent with previous investigations of Abdelsadek et al. [29], who reported that the higher concentration of basic sites in NiMgAl hydrotalcite samples enhanced the catalytic activity.

The first observation is that the hydrotalcite phases exhibited a notable catalytic activity with respect to the reaction of the decomposition of isopropanol even at low reaction temperature compared to other materials like spinel ferrites which are only active beyond 200 °C [38]. The conversion of isopropanol in both formulations is influenced by the rise in the temperature of reaction. The increase in the reaction temperature results in an increase in the transformation of isopropanol to reach at 250 °C the maximum conversion. The isopropanol conversion for the sample NiMgAl-CO$_3$-c resulted higher than that for the binary NiAl-CO$_3$-c. For instance, the conversion of isopropanol at 175 °C reaches 93% and 85% for NiMgAl-CO$_3$ and NiAl-CO$_3$catalysts, respectively. This result reveals that the decomposition of isopropanol is more active over NiMgAl-CO$_3$catalyst.

At higher conversion rate, it is generally no longer the kinetic factors that influence the distribution of the reaction products and it becomes very difficult to give a precise meaning to the observed selectivity. The trends can only be established by

extrapolation of the results obtained at low conversion rate and it is for this purpose
that the reaction has been studied at temperatures lower than or equal to 250 °C.

The isopropanol transformation on NiMgAl-CO$_3$ and NiAl-CO$_3$ catalysts lead to
only acetone and propylene, whereas di-isopropyl ether was not detected. Acetone,
product of the dehydration reaction of isopropanol, needs the presence of basic
sites, while propylene product is formed by the dehydration reaction in the pres-
ence of acid sites. The literature results indicate that the dehydration of the alcohol
to acetone is able of revealing the basic character of the catalysts. However, this last
point is still controversial, because the acetone formation can also involve an oxida-
tion–reduction mechanism, particularly at low temperatures [21, 39]. The activity of
the isopropanol transformation shows that the acetone formation increases with the
rise of the temperature reaction and it is favored by the presence of Mg in the HDL
structure (NiMgAl-CO$_3$-c).

Role of Mg and Al in the hydrotalcite-derived catalysts

According to the literature, a study about vanadium oxides supported on hydrotalcite
type (V/MgAl, with different amounts of Mg (1.00, 0.89 and 0.50) was tested for
isopropanol transformation reaction. It showed that the sample with the largest con-
tent of Mg produced mainly acetone due to the presence of basic sites. Conversely,
the catalyst with the largest amount of Al (i.e., V/Mg0.50Al) enhanced the forma-
tion of propylene due to the presence of acid sites. Vanadium also contributed to the
generation of further acid sites in the catalysts, thereby increasing the conversion of
isopropanol to propylene [21].

Hydrotalcites with different (Al/Al+Mg) ratios and prepared at different tem-
peratures were also investigated in the isopropanol decomposition [22]. When the
decomposition of isopropanol was carried out over calcined sample (450 °C, 18 h),
both acetone and propylene were observed. These results indicate that the calcined
hydrotalcites exhibit both acid and basic sites [40]. Moreover, calcined hydrotal-
cites have basic sites capable of catalyzing consecutive reactions of acetone such as
aldolic condensation and hydrogen transfer. It must be remarked that on the MgO
prepared catalysts only acetone was detected as reaction product, and no further
reaction of the primarily formed acetone was observed.

Furthermore, the presence of Mg almost inhibits the formation of propylene
regardless of temperature. In addition, the existence of Al promotes a great forma-
tion of propylene due to the creation of new acid sites attributed to the substitution
of Mg^{2+} by Al^{3+}. A study of the catalytic conversion of the isopropanol reported that
V-Mg$_x$Al catalyst with larger amount of Mg generated high selectivity of acetone.
The greatest activity in the production of acetone in V-Mg$_{1.0}$Al catalyst is attributed
to the presence of magnesium (basic sites). The same solid with large amount of Al

a

b

c
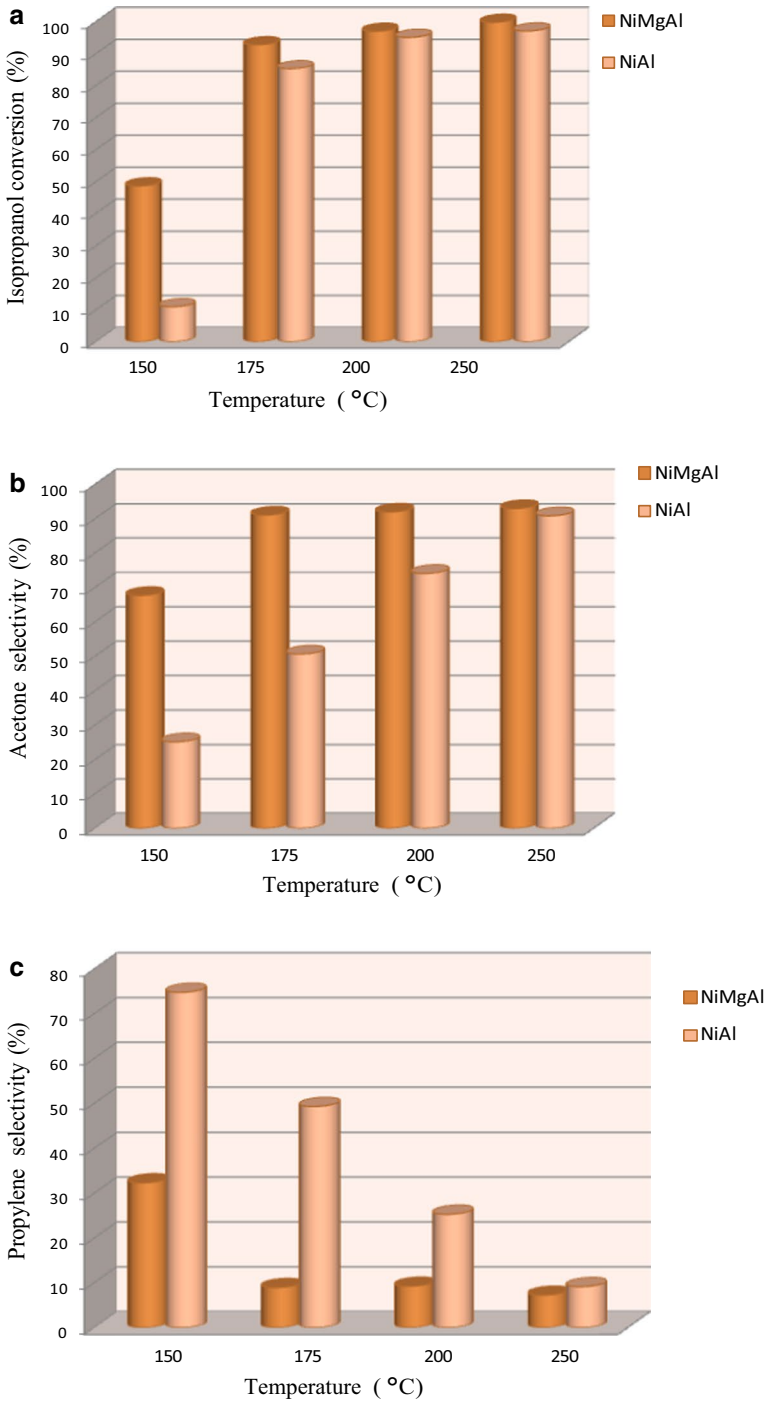
(i.e., V-Mg$_{0.5}$Al) presented more selectivity to propylene due to the presence of a larger number of acid sites [1].

From the structural point of view, the number of defects, and therefore the number of strong basic sites, in the lattice of MgO should be expected to increase (or decrease?) when increasing the amount of Al$_2$O$_3$. On the other hand, an increase in Al should increase the average electronegativity of the solid and thus decreasing the average electronic density of the lattice oxygen since Al is more electronegative than Mg. After calcination, XRD analysis showed the presence of NiO, MgO and Al$_2$O$_3$ for NiMgAl-HTc and NiO and Al$_2$O$_3$ for NiAl-HTc. Since the solids were calcined at temperature (450 °C) higher than the temperature of reaction (150–250 °C), we suggest and expect no change in textural and structural properties during catalytic reaction. According to these factors, the changes in the catalytic activity of the catalysts would be due to the presence of different acid–base and redox properties. In our case NiMgAl-HT and NiAl-HT present different structural and textural properties due to the introduction of Mg into NiAl-HT matrix. They show different catalytic activity and acid–base properties during the catalytic decomposition of isopropanol.

At low reaction temperature (i.e., 150 °C) the NiAl-CO$_3$-c catalyst shows acid sites owing to the main propylene formation. The selectivity to propylene reaches approx. 75%.

Acetone is the only major product obtained for the two catalysts but by increasing the reaction temperature, an evolution of basic sites appeared on the surface of this sample to favor the acetone production so that the selectivity to acetone is 25.2% at 150 °C and increases up to 91% at 250 °C, respectively.

Table 5 (or Fig. 12) shows the selectivity ratio (R) between acetone and propylene: ($R = \frac{\text{Acetone selectivity}}{\text{Propylene selectivity}}$) for the samples and at different temperatures of the reaction.

Except for NiAl-CO$_3$-c catalyst at 150 °C in, the selectivity ratio (R) resulted higher than 1 in both formulations (i.e., NiMgAl-CO$_3$ and NiAl-CO$_3$). Note that the ratio R is more important for NiMgAl-CO$_3$, this result reveals clearly that the acetone is the predominant product owing to the significant basic properties of the sample NiMgAl-CO$_3$-c. The difference in catalytic activity between NiMgAl-CO$_3$-c and NiAl-CO$_3$-c is related to textural and structural properties of the two solids since the crystallite size of NiO changes with the catalyst formulation (Table 5).

According to the literature [29, 36], NiMgAl-derived hydrotalcite catalyst shows higher activity than NiAl catalyst in the hydrogen generation via dry reforming of methane [20], an opposite trend was observed for CoMgAl and CoAl catalysts

Table 5 Selectivity ratio to acetone and propylene with structural parameters in the presence of the samples NiMgAl-CO$_3$-c and NiAl-CO$_3$-c catalysts

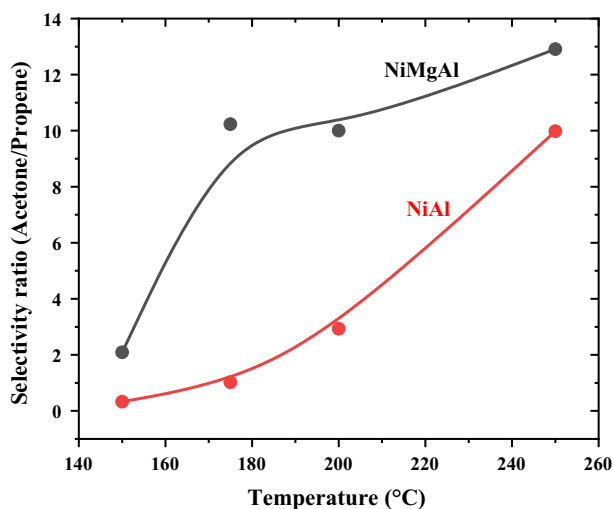| Catalyst	XRD phases	Crystallites size (Å)	Surface area (m^2/g)	$R = \frac{\text{Acetone selectivity}}{\text{Propylene selectivity}}$				
				T (°C)	150	175	200	250
NiMgAl-CO$_3$-c	NiO, MgO	25.22	169	–		2.09	10.23	10.00	12.91
NiAl-CO$_3$-c	NiO	35	117	–		0.33	1.02	2.93	9.98

Fig. 12 Selectivity ratio to acetone and propylene (R) for the NiMgAl-CO$_3$-c and NiAl-CO$_3$-c catalysts

derived from hydrotalcite [41]. In this work, NiMgAl-CO$_3$-c also presents the best and high catalytic activity in the isopropanol decomposition reaction and acetone production owing to its high surface area and a smaller crystallite size. This finding is due to the presence of Mg in the HDL phases which leads to increase in specific area with dispersive effect, formation of small species and favor strength of basic sites. The results showed a good correlation between the catalytic activity and the presence of basic sites created by the presence of Mg in the matrix NiAl, the interaction between MgO and Al$_2$O$_3$ promotes the formation of suitable basic sites.

The basicity of HDL non-calcined phases is attributed to Bronsted basic sites of HO$^-$ hydroxide group located on the HDL network with weak strength. On the other hand, in the case of the mixed oxides MgAl-O, the strong basic sites, are Lewis type (i.e., O^{2-} and M^{2+}-O$_2$), without excluding the hydroxyl species, whose absorption bands have been observed on the infra-red spectra of the solid calcined at 450 °C.

Conclusions

Two catalysts derived from hydrotalcite (i.e., NiMgAl-CO$_3$-c and NiAl-CO$_3$-c) were successfully prepared by coprecipitation method at pH basic constant (pH 11). After their calcination at 450 °C for 6 h, only single oxides were present in the samples. The characterization of fresh and calcined HDL phases using different methods of physical–chemical analysis, such as SAA, TGA/DTA, XRD, SEM, FTIR and RAMAN exhibited the features of HDL phases. The catalysts were tested for the isopropanol decomposition reaction at different reaction temperatures (150, 175, 200, and 250 °C). The solid NiMgAl-CO$_3$-c demonstrated the best catalytic activity due to the presence of magnesium in the HDL phases structure. The incorporation of Mg into the HDL structure enhances the structural and textural properties so that

a high surface area with a small crystallite size is obtained and strong basic sites are created over NiMgAl-CO$_3$-c. To summarize, the study of the catalytic activity of isopropanol transformation showed that the catalytic performances and basic properties vary according to the following order: NiMgAl-CO$_3$-c > NiAl-CO$_3$-c.

References

1. F. Cavani, F. Trifirò, A. Vaccari, Catal. Today **11**, 173 (1991)
2. S. Miyata, T. Kumura, Chem. Lett. **2**, 843 (1973)
3. M.R. Othman, Z. Helwani, W.J.N. Fernando, Appl. Organomet. Chem. **23**, 335 (2009)
4. A. Vaccari, Catal. Today **41**, 53 (1998)
5. J.-M. Lavoie, Front. Chem. **2**, 1 (2014)
6. Z. Abdelsadek, M. Sehailia, D. Halliche, V.M. Gonzalez-Delacruz, J.P. Holgado, K. Bachari, A. Caballero, O. Cherifi, J. CO2 Util. **14**, 98 (2016)
7. Z. Abdelssadek, K. Bachari, A. Saadi, O. Cherifi, D. Halliche, Res. Chem. Intermed. **41**, 1757 (2013)
8. P. Gao, R. Xie, H. Wang, L. Zhong, L. Xia, Z. Zhang, W. Wei, Y. Sun, J. CO2 Util. **11**, 41 (2015)
9. L. Cocheci, P. Barvinschi, R. Pode, E. Popovici, E. Seftel, Chem. Bull. POLITEHNICA Univ. Timisoara **55**, 40 (2010)
10. C. Forano, T. Hibino, F. Leroux, C. Taviot-Guého, Dev. Clay Sci. **1**, 1021 (2006)
11. D. Haffad, A. Chambellan, J.C. Lavalley, J. Mol. Catal. A Chem. **168**, 153 (2001)
12. J.C. Luy, J.M. Parera, Appl. Catal. **26**, 295 (1986)
13. E. Ortiz-Islas, T. López, J. Navarrete, X. Bokhimi, R. Gómez, J. Mol. Catal. A Chem. **228**, 345 (2005)
14. K. Von Tanabe, M. Misono, Y. Ono, H. Hattori, *Angewandte Chemie*, vol. 103 (1) (Elsevier, Amsterdam, 1989), pp. 114–115
15. J.M. Vohs, M.A. Barteau, Surf. Sci. **221**, 590 (1989)
16. X. Gu, J. Ge, H. Zhang, A. Auroux, Thermochim. Acta **451**, 84 (2006)
17. G.C. Bond, S.F. Tahir, Appl. Catal. **71**, 1 (1991)
18. I.E. Wachs, Chem. Eng. Sci. **45**, 2561 (1990)
19. T. Nakatsuka, K. Hitoshi, Y. Shinzo, K. Shinzo, Bull. Chem. Soc. Jpn. **52**, 2449 (1979)
20. G. Fornasari, M. Gazzano, D. Matteuzzi, F. Trifirò, A. Vaccari, Appl. Clay Sci. **10**, 69 (1995)
21. D. Meira, G. Cortez, W. Monteiro, J. Rodrigues, Braz. J. Chem. Eng **23**, 351 (2006)
22. A. Corma, V. Fornes, F. Rey, J. Catal. **148**, 205 (1994)
23. A. Bhattacharyya, V. Chang, D. Schumacher, Appl. Clay Sci. **13**, 317 (1998)
24. A. Monshi, M.R. Foroughi, M.R. Monshi, World J. Nano Sci. Eng. **02**, 154 (2012)
25. F.T.L. Muniz, M.A.R. Miranda, C. Morilla dos Santos, Acta Crystallogr. A Found. Adv. **72**, 385 (2016)
26. D. Tichit, C. Gérardin, R. Durand, B. Coq, Top. Catal. **39**, 89 (2006)

27. E. Kanezaki, Solid State Ion. **106**, 279 (1998)
28. M. Crivello, C. Pérez, J. Fernández, G. Eimer, E. Herrero, S. Casuscelli, E. Rodríguez-Castellón, Appl. Catal. A Gen **317**, 11 (2007)
29. Z. Abdelsadek, J.P. Holgado, D. Halliche, A. Caballero, O. Cherifi, S. Gonzalez-Cortes, P.J. Masset, Catal. Lett. **151**, 2696 (2021)
30. J. Pérez-Ramırez, G. Mul, J. Moulijn, Vib. Spectrosc. **27**, 75 (2001)
31. C. Forano, U. Costantino, V. Prévot, C.T. Gueho, *J. Mater*, vol. 5 (Elsevier, Amsterdam, 2013), pp. 745–782
32. M. Nawfal, C. Gennequin, M. Labaki, B. Nsouli, A. Aboukais, E. Abi-Aad, Int. J. Hydrog. Energy **40**, 1269 (2015)
33. P. Bera, M. Rajamathi, M. Hegde, P.V. Kamath, Bull. Mater. Sci. **23**, 141 (2000)
34. K.L. Erickson, T.E. Bostrom, R.L. Frost, Mater. Lett. **59**, 226 (2005)
35. J.T. Kloprogge, D. Wharton, L. Hickey, R.L. Frost, Am. Mineral. **87**, 623 (2002)
36. X. Zhang, L. Zhang, H. Peng, X. You, C. Peng, X. Xu, W. Liu, X. Fang, Z. Wang, N. Zhang, X. Wang, Appl. Catal. B Environ. **224**, 488 (2018)
37. A.C.C. Rodrigues, C.A. Henriques, J. Mater. Res. **6**, 563 (2003)
38. R. Benrabaa, H. Boukhlouf, A. Löfberg, A. Rubbens, R.-N. Vannier, E. Bordes-Richard, A. Barama, J. Nat. Gas Chem. **21**, 595 (2012)
39. A. Gervasini, J. Fenyvesi, A. Auroux, Catal. Lett. **43**, 219 (1997)
40. A.L. McKenzie, C.T. Fishel, R.J. Davis, J. Catal. **138**, 547 (1992)
41. Z. Abdelsadek, P. Chaudhari, J.P. Holgado, F. Bali, D. Hallcihe, O. Cheifi, S. Gonzalez-Cortes, P.J. Masset, I.O.P. Conf, Ser. Earth Environ. Sci. **880**, 1 (2021)